Journal of Applied Electrochemistry **33**: 863–873, 2003.

Laminar and turbulent mass transfer simulations in a parallel plate reactor[☆]

G. NELISSEN*, B. VAN DEN BOSSCHE, J. DECONINCK, A. VAN THEEMSCHE and C. DAN
Vrije Universiteit Brussel TW/ETEC, Pleinlaan 2, B1050 Brussels, Belgium
*(*author for correspondence, e-mail: gnelisse@vub.ac.be)*

Received 24 October 2002; accepted in revised form 2 April 2003

Key words: high Schmidt number, k—ω model, multi-ion mass transfer, parallel plate reactor, turbulence

Abstract

Laminar and turbulent mass transfer in a parallel plate reactor at high Schmidt number obtained from numerical simulation is compared with literature data. In a first step, the fluid flow is determined numerically in the reactor by solving the Navier–Stokes equations. For turbulent flow, a low Reynolds number k—ω model is used to calculate the turbulent viscosity. Using the obtained flow field and turbulent viscosity, the current density distribution is calculated for different flow velocities by solving the equations describing the transport of multiple ions due to diffusion, convection and migration. For the laminar case, a very good agreement with literature data is obtained. For turbulent flow, different numerical models for turbulent mass transfer are proposed in the literature. A detailed study of the behaviour close to the wall of these different turbulence models is presented, together with a comparison of the calculated results with literature correlations. This allows identification of the benefits and disadvantages of each of the turbulence models for the numerical calculation of mass transfer at high Schmidt numbers in a parallel plate reactor.

List of symbols

C, C_l	concentration, concentration of ion l (mol m^{-3})
$C_{\text{bulk}}, C_{l,\text{bulk}}$	bulk concentration, bulk concentration of ion l (mol m^{-3})
d	half height of the channel (m)
d_{h}	hydraulic diameter, equal to 4 d (m)
$D_{\text{mol}}, D_{l,\text{mol}}$	molecular diffusion coefficient, molecular diffusion coefficient of ion l (m^2 s^{-1})
$D_{\text{t}}, D_{l,\text{t}}$	turbulent diffusion, turbulent diffusion of ion l (m^2 s^{-1})
E_0	equilibrium potential (V)
F	Faraday constant (96 487 C mol^{-1})
i, j	summation indices
J	current density (A m^{-2})
k	turbulent kinetic energy per unit mass (m^2 s^{-2})
k_m	mass transfer coefficient (m s^{-1})
L	length of the electrode (m)
n	number of electrons involved in a reaction
$\vec{n}$	normal (m)
$N_{il}, \vec{N}_l$	(components of) mass transfer flux of ion l (mol m^{-2} s^{-1})
p	static pressure (Pa)
R	universal gas constant (8.3143 J mol^{-1} K^{-1})
R_l	production rate of ion l (mol m$^{-3}s^{-1}$)
Re	Reynolds number
Re_{t}	turbulent Reynolds number
S	surface of the electrode (m^2)
Sc	Schmidt number
Sc_{t}	turbulent Schmidt number
Sh	Sherwood number
t	time (s)
S_{ij}	strain rate (s^{-1})
t_{ij}	viscous stresses (kg m^{-1}s^{-2})
T	absolute temperature (K)
u_i'	fluctuating velocity components (ms^{-1})
u_l	mobility of ion l (m^2 mol J$^{-1}s^{-1}$)
u_τ	friction velocity (m s^{-1})
U_i	components of velocity vector $\vec{v}$ (m s^{-1})
x_i	space coordinates (m)
z_l	charge of ion l

Greek symbols

δ_{ij}	chronecker delta
η	overpotential (V)
μ	dynamic viscosity (kg m^{-1}s^{-1})
ν	kinematic viscosity (m^{2}s^{-1})
ν_{t}	turbulent viscosity (m^{2}s^{-1})
ρ	density of the electrolyte (kg m^{-3})
τ_{ij}	Reynolds stresses (kg m$^{-1}s^{-2}$)

[☆] This paper was originally presented at the 6th European Symposium on Electrochemical Engineering, Düsseldorf, Germany, September 2002.

τ_{wall}	surface shear stress (kg $m^{-1}s^{-2}$)
Φ	electrical potential of electrolyte (V)
Φ_m	electrical potential of electrode (V)
ω	specific dissipation rate (s^{-1})
Ω_{ij}	mean rotation tensor (s^{-1})

1. Introduction

One of the most important factors in the operation of plating reactors is the local mass transfer, which is mainly determined by the electrolyte flow in the reactor. To optimize a plating reactor, an accurate prediction of the local mass transfer and thus the fluid flow is needed. This paper presents a numerical model to calculate the laminar and turbulent fluid flow and mass transfer in arbitrary shaped reactors.

Because both the flow and the mass transfer are well defined and documented, the parallel plate geometry is a very suitable test case for a turbulent flow solver and turbulent mass transfer calculations. Therefore, in order to estimate the validity and accuracy of turbulent mass transfer calculations, different models are used to calculate the turbulent mass transfer in a parallel plate reactor. These calculations are compared with a correlation obtained from measurements [1, 2].

A k—ω model is used to calculate the turbulent viscosity in order to solve the Reynolds averaged Navier–Stokes equations describing the turbulent fluid flow. The low Reynolds version of the k—ω model, which includes this 'combination' of k—ω and k—ϵ approaches, presented in the work of Wilcox [3] has been implemented. To evaluate the performance of this model, the calculations of the flow and turbulence parameters for a channel are compared with 'direct numerical simulation' (DNS) [4, 5].

Steady-state numerical computations for the non-simplified multi-ion transport model, including diffusion, migration, convection and chemical and electrode reactions, have been presented by several authors. For example, Georgiadou and Alkire presented results in a complex geometry and flow field, based on the 'finite difference method' (FDM) in combination with an upwind scheme for the convection [6, 7]. Also Volgin and Davidov [8, 9] have performed multi-ion calculations using the finite difference method. Most of the presented examples are rather theoretical, but some interesting comments on the stability and solution speed of the multi-ion equations are made. A method based on the 'finite volume method' (FVM) was presented by Bortels [10] and Van den Bossche [11]. This approach was the basis for the work presented in this paper. The results presented by the authors mentioned above show the possibilities of the multi-ion transport and reaction model to predict current density, potential and concentration distributions in artificially shaped electrochemical reactors. However, all these calculations are limited to laminar flow conditions.

Several authors [12–16] present results of mass transfer in electrochemical reactors with turbulent flow. Most of them are based on a boundary integral method to solve for the boundary layer or only solve the convection–diffusion equation, including the turbulent diffusion, for the limiting current situation. To the authors knowledge, none of these calculation use the full multi-ion model including the effects of turbulence on the mass transfer. Gurniki [17] studied the use of 'large eddy simulations' (LES) for predicting turbulent mass transfer in a parallel plate reactor. In that work also the turbulent fluctuations of the concentration are modelled. However, the influence of migration on the mass transfer is neglected and the presented approach is only valid for binary electrolytes.

2. Turbulence model

2.1. *Reynolds averaged Navier–Stokes Equations*

For engineering applications, one is generally only interested in the statistical values of the random variations encountered in turbulence. Therefore, the study of turbulent flow usually involves an averaging of the equations describing the flow. This averaging process, as explained in detail in [3], leads to the 'Reynolds averaged Navier–Stokes' (RANS) equations.

The equations describing the turbulent fluid flow are the incompressible RANS equations:

$$\frac{\partial U_i}{\partial x_i} = 0 \tag{1}$$

$$\rho \frac{\partial U_i}{\partial t} + \rho U_j \frac{\partial U_i}{\partial x_j} = -\frac{\partial p}{\partial x_i} + \frac{\partial (t_{ji} + \tau_{ji})}{\partial x_j} \tag{2}$$

with U_i the mean velocity components, p the mean pressure, t the time, ρ the density, t_{ij} the mean viscous stresses given by

$$t_{ij} = 2\mu S_{ij} \tag{3}$$

with μ the molecular viscosity and S_{ij} the mean strain rate given by

$$S_{ij} = \frac{1}{2}\left(\frac{\partial U_i}{\partial x_j} + \frac{\partial U_j}{\partial x_i}\right) \tag{4}$$

By analogy with the viscous stresses, the Boussinesq eddy–viscosity approximation (linear model) states that the turbulent stresses (Reynolds stresses) τ_{ij} are given by

$$\tau_{ij} = 2\mu_t S_{ij} - \frac{2}{3}\rho k \delta_{ij} \tag{5}$$

with μ_t the turbulent viscosity, which in contrast to the molecular viscosity, is not a property of the fluid but of the flow. The variable k is the specific turbulent kinetic

energy equal to half of the sum of the squares of the fluctuating velocity components:

$$k = \frac{1}{2} u_i' u_i' \tag{6}$$

The factor 2/3 in Equation 5 only holds for the 3D case. In two-dimensions, this factor becomes 1.

Equations 1 and 2 are identical in form to the laminar Navier–Stokes equations except for the additional turbulent Reynolds stresses which appear in the stress tensor terms.

The numerical treatment of the RANS and the turbulence model is based on the work of Waterson [18]. A residual distribution approach ('multidimensional upwind method', MDUM) is used.

2.2. *k—ω model*

The equations describing the low-Reynolds version of the Wilcox k—ω model are presented is the appendix.

An important aspect of the numerical treatment of the k—ω model is the need to guarantee that the turbulence variables (k and ω) remain positive and finite at all time during the solution process. The convective terms in Equations 28 and 29 are discretized using MDUM. The scalar N-scheme is used to ensure the positive definiteness of both k and ω. The diffusive terms are treated with the standard Galerkin finite element method.

3. Mass transfer models

3.1. *Convection–diffusion model*

When migration is neglected, the stationary convection–diffusion equation including turbulent mass transfer [19], can be written as

$$U_i \frac{\partial C}{\partial x_i} = \frac{\partial}{\partial x_i}\left[(D_{\text{mol}} + D_{\text{t}})\frac{\partial C}{\partial x_i}\right] \tag{7}$$

with U_i the velocity components calculated as described above, C the concentration, D_{mol} the molecular diffusion constant and D_{t} the turbulent diffusion. By analogy to the linear approximation for the Reynolds stresses, the mass transfer flux due to turbulence can be written as $-D_{\text{t}}\partial C/\partial x_i$. Similar as for the fluid flow, a model needs to be proposed to calculate D_{t}.

This model describes the mass transfer in binary electrolyte or allows a fast calculation of the limiting current for one ion, by setting the concentration of the reacting ion to zero at the electrode(s).

For mass transfer one can define the following dimensionless numbers:

$$Sc = \frac{\nu}{D_{\text{mol}}} \tag{8}$$

the Schmidt number, equivalent to the Prandtl number in heat transfer, describing the ratio between the viscosity and the molecular diffusion constant, and

$$Sc_{\text{t}} = \frac{\nu_{\text{t}}}{D_{\text{t}}} \tag{9}$$

the turbulent Schmidt number, equivalent to the turbulent Prandtl number, describing the ratio between the turbulent viscosity and the turbulent diffusion.

The boundary conditions are $C = C_{\text{bulk}}$ on the inlet(s) and, at the limiting current, $C = 0$ on the cathode(s). On all the other boundaries, the natural boundary condition $\partial C/\partial \vec{n} = 0$ is imposed.

3.2. *Multi-ion transport and reaction model*

For each species l one can state that at each point in the solution, the change of concentration is equal to the net input plus the local production (or reduction) due to chemical reactions. In differential form this is described as follows:

$$\frac{\partial C_l}{\partial t} = -\frac{\partial}{\partial x_i}(N_{il}) + R_l \tag{10}$$

with N_{il} the components of $\vec{N}_l$ the mass transfer flux. The production per unit volume R_l involves homogeneous chemical reactions in the bulk of the solution, but no electrode reactions. In this paper no homogeneous reactions are considered, in which case the term R_l equals zero.

The flux of each dissolved species l (no summation over l) due to molecular diffusion, convection, migration and turbulent diffusion is given by:

$$N_{il} = -(D_{l,\text{mol}} + D_{l,\text{t}})\frac{\partial C_l}{\partial x_i} + C_l u_i - z_l u_l F C_l \frac{\partial \Phi}{\partial x_i} \tag{11}$$

with C_l the molar concentration (mol m^3), z_l the charge, u_l the mobility (m^2 mol J^{-1} s^{-1}), Φ the electrical potential (V), $D_{l,\text{mol}}$ the diffusion coefficient (m^2 s^{-1}), $D_{l,\text{t}}$ the turbulent diffusion (m^2 s^{-1}), U_i the velocity of the solvent (m s^{-1}), and F the faradaic constant.

As this is a first attempt to include the effects of turbulence on the multi-ion mass transfer the influence of the turbulent fluctuations on the electrical potential is neglected.

The unknowns in the mass conservation equations are the ion concentrations and the potential in each point of the solution. Hence an additional equation, the electroneutrality condition, is added to the mass conservation equations:

$$\sum_{l=1}^{I} z_l C_l = 0 \tag{12}$$

This equation expresses that the electric conductivity is too large for free charges to exist.

The imposed boundary conditions are as follows:
(i) at insulators, symmetry planes and outlet

$$\frac{\partial U}{\partial \vec{n}} = 0, \qquad \frac{\partial C_l}{\partial \vec{n}} = 0 \tag{13}$$

(ii) at inlet(s)

$$C_l = C_{l,\text{bulk}} \tag{14}$$

(iii) at electrode(s)

$$\vec{N}_l \cdot \vec{n} = 0 \tag{15}$$

for non-reacting ions.

For the active ions, the flux is related to the speed of the electrode reactions. The driving force of these electrode reactions is the overpotential:

$$\eta = \Phi_\text{m} - \Phi - E_0 \tag{16}$$

that is, the difference between the (imposed) potential on the electrodes Φ_m and the electrolyte potential Φ at the other side of the double layer, with respect to the equilibrium potential E_0. In general the values of Φ_m and Φ can vary along the electrode surface, respectively due to the ohmic voltage drop in the electrode and to the nonuniform current density distribution. The overpotential η depends on the local current density and on the local ion concentration at the electrode surface. Often a Butler–Volmer equation is used to describe this dependency $J = f(\eta, C_k)$. Assuming further that only one reaction:

$$A^{n+} + n\text{e}^- \rightleftharpoons A \downarrow \tag{17}$$

takes place, the flux for ion A^{n+} is written as

$$\vec{N}_{A^{n+}} \cdot \vec{n} = \frac{J}{nF} \tag{18}$$

and the current density of the reaction is given by the following Butler–Volmer expression:

$$J = J_{0,\text{a}} \text{e}^{\alpha_\text{a} n\eta F/RT} - J_{0,c} C_{A^{n+}} \text{e}^{-\alpha_\text{c} n\eta F/RT} \tag{19}$$

In this paper, an electrochemical system with the parameters $J_{0,\text{a}} = 10$ A m^{-2}, $J_{0,\text{c}} = 1$ A m^{-2} mol^{-1}, $\alpha_\text{a} = 0.75$, $\alpha_\text{c} = 0.25$, $n = 2$ is considered.

On the anode, an infinitely fast electrode reaction is considered, so that the overpotential can be neglected (primary distribution).

Combination of these electrode kinetics with the multi-ion model gives a closed system of equations, in which the overpotential as a driving force for the electrode reactions is included in a straightforward way. When the potential different between anode and cathode is imposed, as is done in reality, the potential, concentration and current density distribution in the reactor can be calculated without any further approximations or assumptions.

3.3. *Turbulent mass transfer models*

Four models for the turbulent diffusion are commonly proposed for turbulent high Schmidt number mass transfer calculations.

The turbulent diffusion is neglected based on the idea that the mass transfer boundary layer is so thin that it is fully encompassed in the viscous sublayer of the turbulent fluid flow. There are some strong arguments that this assumption is too simple and does not give very good predictions for general flow cases. However, this assumption is valid if the length of the electrode is small ($L\sqrt{\tau_\text{Wall}/(\mu\nu)} = L^+ < 700$) as demonstrated in [16, 20].

The model Sc_t = constant is the straightforward extrapolation of what is generally done in turbulent heat transfer (see [12, 21]. A typical value used in heat transfer is $Pr_\text{t} = 0.71$.

More elaborated models consider the dependence of Sc_t on global quantities of the flow ($Re, Sc, \ldots$). This implies that this approach is only applicable for a limited number of standard cases (parallel plate, pipe, ...). Furthermore, the dependence of Sc_t differs from author to author [15, 22] and generally does not take account of any local effects of the flow on the mass transfer. For example based on measurements of mass transfer coefficients in circular pipe flow [23], Rosen [15] suggests:

$$Sc_t = \frac{0.0014[1 - \text{e}^{(-0.5\,Re_\text{mod}^{1/2})}]}{0.001\,242\,Sc^{-0.112}} \tag{20}$$

with $Re_\text{mod} = 0.001(Re - 3000)$.

Several different algebraic turbulence models for D_t have been presented [14, 24, 25], most of them based on one set of measurements. Most models start from the observation, both theoretical and experimental, that the turbulent diffusion varies with y^3 close to the wall. A typical example is the model of Aravinth [14]. He proposes:

$$\frac{D_\text{t}}{\nu} = \frac{0.0007\,y^{+3}}{(1 + 0.004\,05\,y^{+2})^{1/2}} \qquad 0 < y^+ < 30, \qquad Sc \geqslant 1 \tag{21}$$

The law of the wall suggests that Equation 21 is universal for all turbulent boundary layers [14].

Also some attempts exist to use an explicit algebraic turbulent stress transport model for passive scalar variables [26, 27]. Although these models seem very promising, they are much more complicated then the models presented above, and give no guarantee of more accurate results. Therefore, they are not used in this work.

Recently, some authors [13, 28] used DNS or LES for the turbulent flow and scalar transport in a channel to

validate the different turbulence models described above. They found that the turbulent Schmidt number is close to one for $y^+ > 5$. Close to the wall, D_t was found to vary with y^{+3}. The algebraic model:

$$\frac{D_t}{\nu} = 0.000\,494\ y^{+3.38}, \qquad Sc = 2400 \tag{22}$$

as identified by Papavassiliou [29] from DNS calculations, coincides very well with the model of Aravinth, especially close to the wall. Therefore only the algebraic model governed by Equation 21 is used in the calculations.

4. Results and discussion

4.1. *Turbulent flow in a parallel plate reactor*

As a first test case the turbulent flow in a parallel plate reactor (channel) is calculated and validated with literature results. The reference results are obtained from DNS and presented in [4, 5]. Figure 1 shows the geometry under investigation. The half-height of the channel, (d) is 0.005 m. The Reynolds number, based on the average inlet velocity, the half-height of the cell and the kinematic viscosity (10^{-6} m^2 s^{-1} for water) is 3300.

The computational mesh, partly shown in Figure 2, contains 29 770 triangles and 14 886 points. The first element is at a normal distance of $y^+ = 0.05$ from the wall. This figure also shows the calculated turbulent velocity profile.

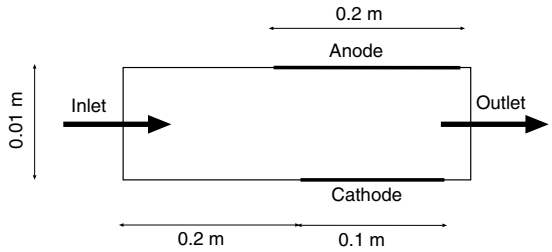

Fig. 1. Schematical overview of the reactor geometry.

Figure 3 compares the developed velocity profile with the reference solution. A agreement, similar to other low-*Re* k—ω implementations [3] is observed. For the viscous sublayer ($y^+ \leqslant 10$, which contains the turbulent diffusion layer) the agreement is very good, for the log layer ($y^+ \geqslant 10$) the profiles differ. In Figure 4, the dimensionless turbulent kinetic energy profile is shown. Quite a good agreement with the reference solution is obtained, especially close to the wall. These results are in perfect agreement with the predictions of other implementations (e.g., [3]) of the Low Reynolds Number k—ω model and form the basis for all subsequent mass transfer calculations.

4.2. *Turbulent mass transfer in a parallel plate reactor at high Schmidt number*

To investigate the turbulent mass transfer in a parallel plate reactor, the limiting current is calculated for different flow rates and compared with correlations found in literature. These correlations are measured in

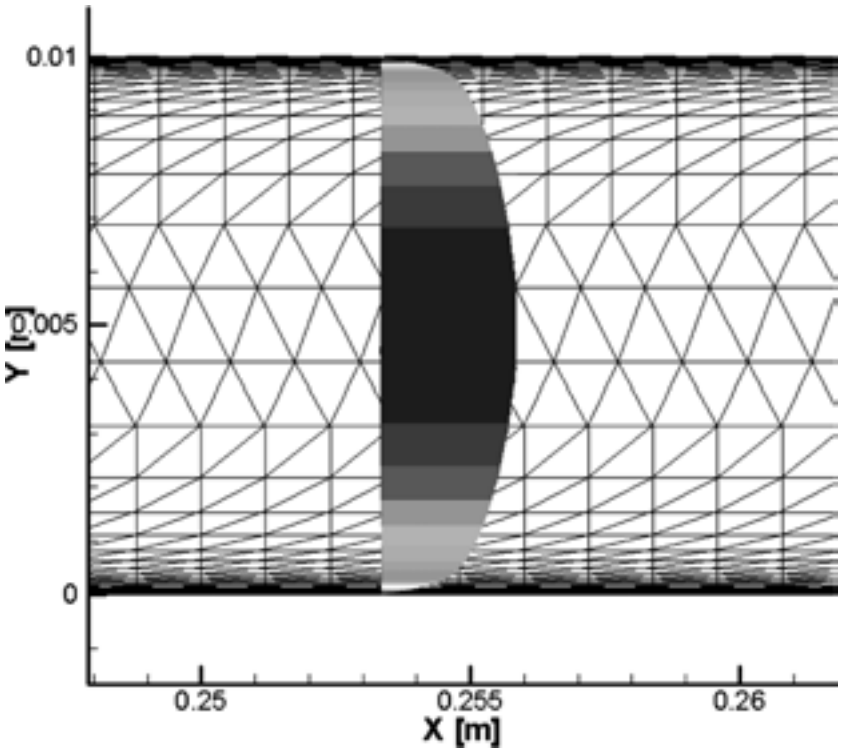

Fig. 2. Flow field and grid in the channel reactor.

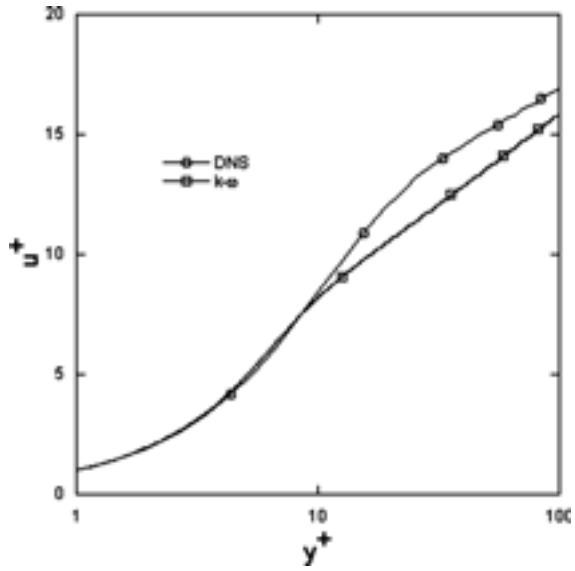

Fig. 3. Dimensionless velocity profile. Key: (○) DNS; (□) k—ω.

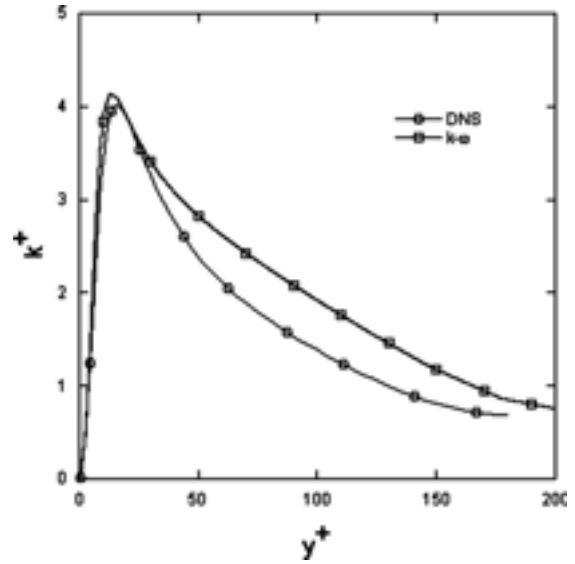

Fig. 4. Dimensionless turbulent kinetic energy profile. Key: (○) DNS; (□) k—ω.

limiting current density conditions and are presented in dimensionless form as $Sh = f(Re, Sc)$. The Sherwood number, defined as

$$Sh = \frac{k_m d}{D_{mol}} \tag{23}$$

and is related to the limiting current by

$$Sh = \frac{I_{lim} d}{S\ n\ F\ C_{bulk}\ D_{mol}} \tag{24}$$

4.2.1. *Correlations*

For mass transfer in laminar flow Pickett [2] proposes the correlation

$$Sh = 2.33 \left(\frac{Re\ Sc\ d}{L} \right)^{1/3} \tag{25}$$

Other authors [30, 31] use analytical solutions or numerical simulations to obtain the limiting current density distribution in channel flow cells.

For turbulent mass transfer in channel cells several correlations are proposed [1]. The most commonly used is the Chilton–Colburn analogy:

$$Sh = 0.023\, Re^{0.8}\, Sc^{1/3} \tag{26}$$

According to Pickett [2], this correlation is only valid for an electrode of length greater than 12.5 hydraulic diameters. Pickett suggests the following empirical correlation for electrodes with length L smaller than 7.5 hydraulic diameters (d_h) in developing mass transfer conditions:

$$Sh = 0.145\, Re^{2/3}\, Sc^{1/3} \left(\frac{d_h}{L} \right)^{1/4} \tag{27}$$

4.2.2. *Calculations*

When performing the calculations, different turbulent mass transfer models yield a different distribution of the turbulent diffusion normal to the fixed wall (electrode). Figure 5(a) and (b) show these fully developed distributions for $Sc_t = 1$ ($D_t = \nu_t$) and for the algebraic model presented in Section 3.3 for a flow at $Re = 8333$ and $Sc = 1714$. Figure 5(a) shows the turbulent diffusion throughout the buffer layer ($y^+ \leqslant 50$) and Figure 5(b) is a zoom of the behaviour of the turbulent diffusion in the mass transfer boundary layer ($y^+ \leqslant 5$). From these Figures it is clear that for this example, according to the models used, the molecular diffusion is dominant only for a very small zone near the wall ($y^+ \leqslant 1$). This of course means that neglecting the turbulent diffusion will yield significantly different mass transfer rates. Both models are independent of Sc, which means that neither can accurately predict the mass transfer over a large range of Sc values, unless the turbulent fluctuations of the mass transfer are independent of Sc.

Considering long electrodes, the results of the numerical calculations and the different correlations for laminar and low Reynolds number turbulent flow are shown in Figures 6 and 7. It is clear that a very good agreement between correlations and simulations is obtained for the mass transfer in the laminar flow regime ($Re < 1500$). From the correlations, it can be estimated that the transition from the laminar to the turbulent regime occurs around $Re = 1500$ to 2000. It is however obvious that this transition is not captured accurately by the k—ω turbulence model, a well known problem for most RANS based turbulence models. These standard k—ω models predict transition from laminar to turbulent flow at Reynolds numbers that are up to one order of

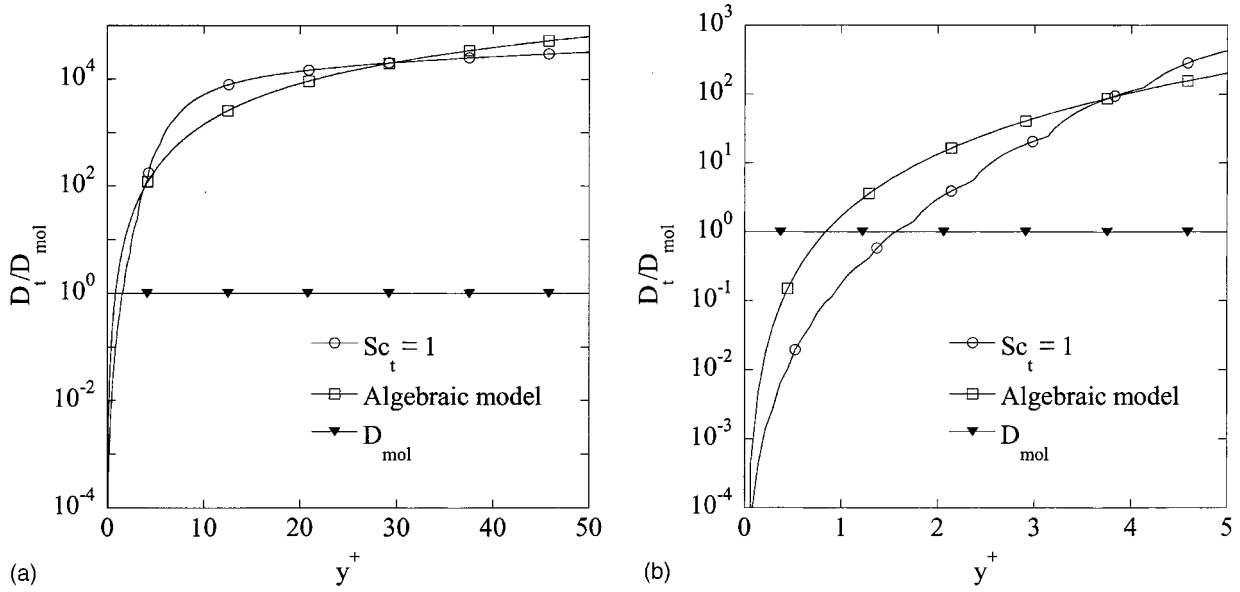

Fig. 5. Turbulent diffusion normal to the wall, $Re = 8333$, $Sc = 1714$ (a) Turbulent diffusion profile, (b) Turbulent diffusion close to the wall. Key: (○) $SC_t = 1$; (□) algebraic model; (▼) D_{mol}.

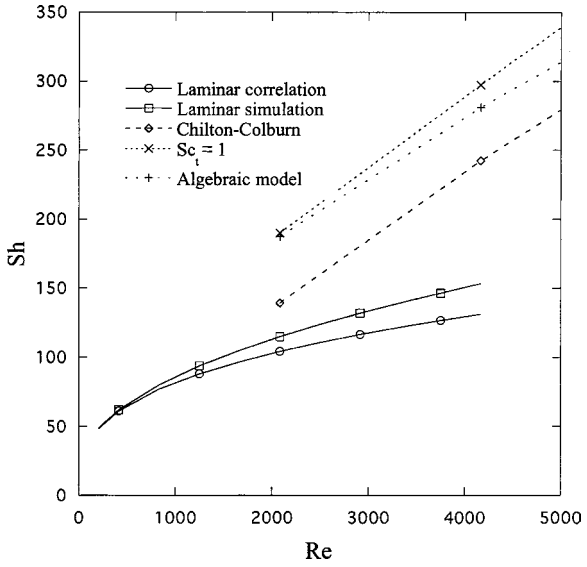

Fig. 6. Sherwood number for different Reynolds numbers; laminar and low Reynolds number turbulent flow, $Sc = 1714$. Key: (○) laminar correlation; (□) laminar simulation; (◇---◇) Chilton–Colburn; (x···x) $Sc_t = 1$; (+---+) algebraic model.

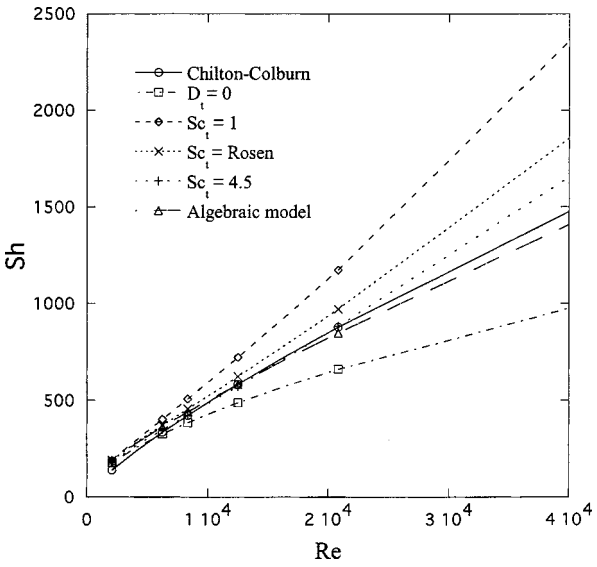

Fig. 7. Sherwood number for different Reynolds numbers; turbulent flow, $Sc = 1714$. Key: (○—○) Chilton–Colburn; (□---□) $D_t = 0$; (◇---◇) $Sc_t = 1$; (x···x) Sc_t = Rosen; (+---+) $Sc_t = 4.5$; (△—△) algebraic model.

magnitude too low, as explained in [3]. Some modifications of the k—ω are therefore proposed by Wilcox. Even with these modifications, the predictive quality based turbulence models for turbulent mass transfer remains limited for the transition from laminar to turbulent flow.

For turbulent mass transfer, the turbulent mass transfer model has a very large influence on the Sherwood number as presented in Figure 7. It is clear that the assumption $D_t = 0$ (equivalent to $Sc_t = \infty$) underestimates the turbulent mass transfer and that $Sc_t = 1$ overestimates it, when compared with the experimental values from the Chilton–Colburn correlation. The model of Rosen is much better in predicting the turbulent mass transfer in a channel, especially at higher Re numbers. From this it is evident that there should exist a reasonable finite value of Sc_t for which, at least in this test case, the simulation matches the correlation perfectly. With some trial and error, this value was found to be 4.5, for which the corresponding results are also given in Figure 7. Finally, the algebraic turbulent mass transfer model gives very good predictions, as this model is derived from measurements for mass transfer in pipe flow.

In the future, additional tests will be performed in other geometries for a large range of Sc and Re numbers

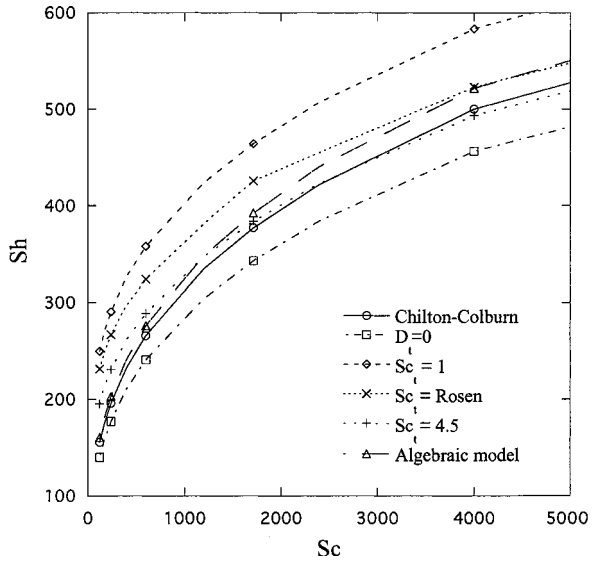

Fig. 8. Sherwood number for different Schmidt numbers; turbulent flow, $Re = 8333$. Key: (○—○) Chilton–Colburn; (□- - -□) $D_t = 0$; (◇- - -◇) $Sc_t = 1$; (x···x) Sc_t = Rosen; (+- - -+) $Sc_t = 4.5$; (△—△) algebraic model.

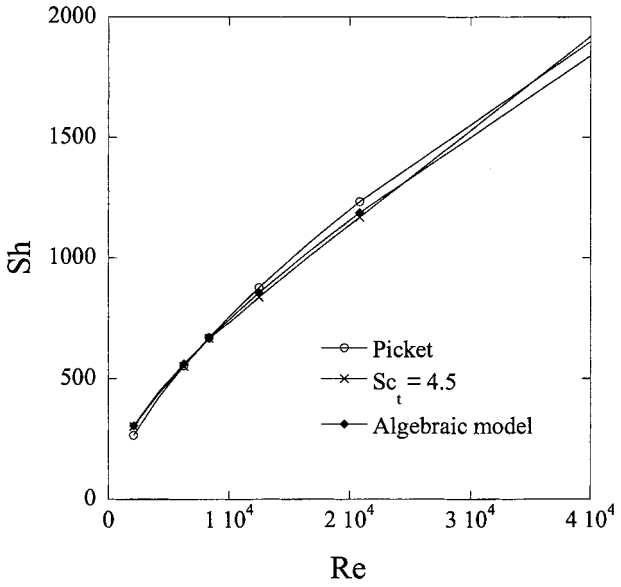

Fig. 9. Short electrode: Sherwood number for different Reynolds numbers; $Sc = 1714$. Key: (○—○) Picket; (x—x) $Sc_t = 4.5$; (◆) algebraic model.

in order to verify the validity and applicability of the different turbulent mass transfer models.

4.3. *Turbulent mass transfer for different Schmidt numbers*

The calculated Sherwood number as a function of the Schmidt number for different turbulent mass transfer models and the Chilton–Colburn correlation are shown in Figure 8.

For these calculations the agreement between measurements and calculations is also best for the algebraic turbulent diffusion model and the $Sc_t = 4.5$ model. For the complete range of Sc, these models predicts the correlation almost perfectly. The model presented by Rosen, whereby the turbulent Schmidt number is related to the Reynolds and Schmidt number, predicts the correlation very well for high values of Sc, but is not so accurate for low Sc values.

4.4. *Turbulent mass transfer in a parallel plate reactor with short electrodes*

Taking $Sc = 1714$, the calculations with electrode length equal to two hydraulic diameters, show a good agreement between the correlation (Equation 27) and the numerical results as is observed in Figure 9. Furthermore, the different mass transfer turbulence models yield the same Sherwood number within 10%. This can be explained by the fact that as the mass transfer boundary layer starts developing at the beginning of the electrode, the boundary layer remains quite small for short electrodes. From Figure 5 it is clear that as long as the turbulent mass transfer boundary layer remains smaller then $y^+ \leqslant 2$ the molecular diffusion is dominant and thus the resulting (turbulent) mass transfer remains independent of the model chosen for the turbulent diffusion. As already proposed by Son and Hanratty [32], this leads to the conclusion that turbulent mass transfer only plays an important role when the electrode are sufficiently long to allow the mass transfer boundary layer to develop until the turbulent mass transfer becomes important.

4.5. *Turbulent mass transfer for multi-ion model for long electrodes*

The turbulent diffusion is assumed to be the same for all ions involved in the multi-ion system. In this paper, the only turbulent diffusion model used for multi-ion calculations is $Sc_t = 1$.

Calculations of the concentration and potential distributions described by the multi-ion model are performed for the (artificial) electrochemical system as shown in Table 1. The only reaction that takes place is the reduction of ion A as described by Equation 19.

The current density distributions along the cathode for different fractions of the limiting current density are shown in Figure 10. The corresponding concentration profiles of the reacting ion at the electrode surface are given in Figure 11. Similar results have been presented for laminar flow by Bortels [10].

Table 1. Properties of the ions

Ion	k	z_k	$C_{k,\text{bulk}}$ mol m^{-3}	$D_k \times 10^{10}$ m^2 s^{-1}
A	1	+2	10	5
B	2	−2	110	4
C	3	+1	200	10

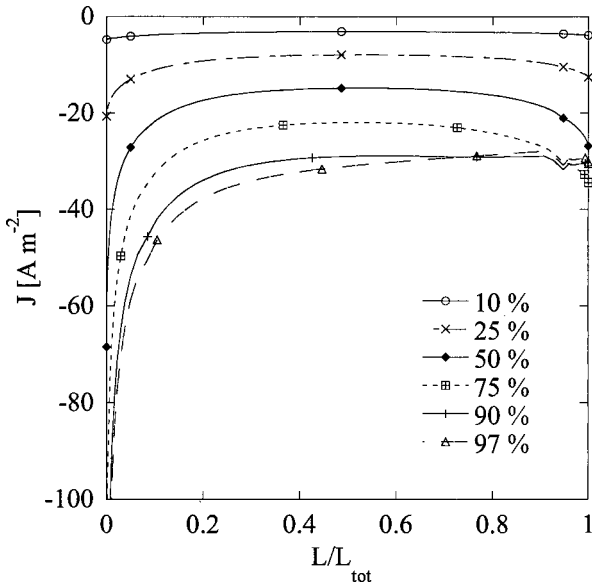

Fig. 10. Current density distribution along the cathode for different fractions of the limiting current, $Re = 8333$ Key: (○—○) 10%; (x– – –x) 25%; (◇– – –◇) 50%; (⊞– – –⊞) 75%; (—|—) 90%; (△– –△) 97%.

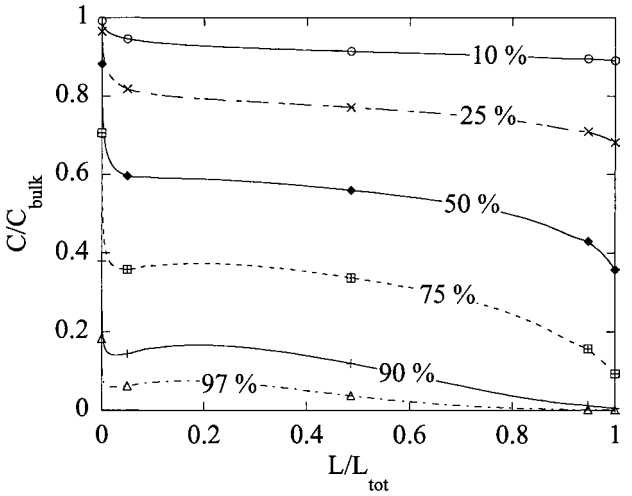

Fig. 11. Concentration profiles of ion A along the cathode for different fractions of the limiting current, $Re = 8333$.

As expected, the downstream part of the cathode reaches the limiting current density regime first, because the electrolyte becomes successively depleted along the cathode. It is important to note that even at 75% of the total limiting current, no part of the cathode is at limiting current. At the leading edge of the cathode, the edge effect (involving a very high current density) will sharply decrease the concentration of the reacting ion. Note also the 'bump' in the concentration profile for the total current between 50% and 97% of the limiting current, similarly as observed in [33] for laminar flow. This is due to competition between the increase in the concentration by diffusion of ions through the boundary layer and decrease in concentration due to the deposition reaction. As long as the boundary layer is quite thin, the diffusive transport will be dominant and the concentration will rise, but at a certain point along the cathode, the boundary layer becomes too thick and the concentration starts decreasing. For the lower currents, the edge effect does not create a concentration gradient large enough to have an increase in concentration due to diffusion. It is clear from Figure 10 that mass transfer only plays an important role at 50% or higher of the limiting current. Hence, it is also expected that the turbulent mass transfer model will have a limited influence on the calculated multi-ion mass transfer. This will be subject of further study.

5. Conclusions

Calculations of turbulent mass transfer in a parallel plate reactor with long and short electrodes were performed and validated using correlations found in literature. Different models for the turbulent diffusion D_t were studied, showing that the algebraic model and the model with $Sc_t = 4.5$ give the best results for a parallel plate reactor with long electrodes. Both neglecting the turbulent diffusion, and extrapolating the turbulent Schmidt number from heat transfer, give unacceptable results, even for this very simple geometry. From the study of a parallel plate reactor with short electrodes it can be concluded that, if the electrode length is short, the turbulent mass transfer can be neglected because the turbulent diffusion remains negligible compared with the molecular diffusion throughout the mass transfer boundary layer. It was demonstrated that this approach to modelling turbulent mass transfer can be extrapolated from the limiting current case to much more general multi-ion calculations. Further research is needed to verify whether these conclusions can be extended to other geometrical configurations and more complex electrochemical systems.

Acknowledgement

The authors express their gratitude to the 'Fonds voor Wetenschappelijk Onderzoek, Vlaanderen' (contract G.0371.97) for financial support of this work.

References

1. A. Averill and H. Mahnood, *Trans. IMF* **74** (1996) 11.
2. D.J. Pickett, 'Electrochemical Reactor Design' (Elsevier, Oxford, 1979).
3. D. Wilcox, 'Turbulence Modeling for CFD' (DCW Industries, 2nd edn, 1998).
4. P. Moin and J. Kim, *J. Fluid Mech.* **155** (1982) 491.
5. N. Mansour, J. Kim and P. Moin, *J. Fluid Mech.* **194** (1988) 15.
6. M. Georgiadou and R. Alkire, *J. Electrochem. Soc.* **141** (1994) 679.
7. M. Georgiadou, *J. Electrochem. Soc.* **144** (1997) 2732.
8. V. Volgin, O. Volgina and A. Davydov, *Comput. Chem.* **411** (2000) 129.

9. V. Volgin and A. Davydov, *Russian J. Electrochem.* **31** (2001) 1197.
10. L. Bortels, J. Deconinck and B.V.D. Bossche, *J. Electroanal. Chem.* **404** (1996) 15.
11. B.V.D. Bossche, L. Bortels, J. Deconinck, S. Vandeputte and A. Hubin, *J. Electroanal. Chem.* **411** (1996) 129.
12. Y. Wang and J. Postlethwaite, *Corros. Sci.* **39** (1997) 1265.
13. I. Calmet and J. Magnaudet, *Phy. Fluids* **9** (1997) 438.
14. S. Aravinth, *Int. J. Heat Mass Trans.* **43** (2000) 1399.
15. C. Rosen and C. Traegaardh, *Chem. Eng. J.* **59** (1995) 153.
16. R. Chalupa, M. Chen, V. Modi and A.C. West, *Int. J. Heat Mass Transfer* **44** (2001) 3775.
17. F. Gurniki, K. Fukagata, S. Zahrai and F. Bark, *J. Appl. Electrochem.* **29** (1999) 27.
18. N. Waterson, 'Flow Simulation at Low Mach Number using a Residual-Distribution Approach', PhD thesis (Technische Universiteit Delft, 2002).
19. A.J. Reynolds, 'Turbulent Flows in Engineering' (J. Wiley & Sons, New York, 1974).
20. D. Shaw and T. Hanratty, *AIChE J.* **23** (1977) 160.
21. S. Nesic, J. Postlethwaite and D. Bergstrom, *Int. J. Heat Mass Transf.* **35** (1992) 1977.
22. M. Behnia, S. Parneix and P. Durbin, *Int. J. Heat Mass Transf.* **41** (1998) 1845.
23. D. Shaw and T. Hanratty, *AIChE J.* **23** (1977) 28.
24. A. Sleicher and R. Notter, *Chem. Eng. Sci.* **26** (1971) 161.
25. S. Martemyanov, E. Skurygin and J. Legrand, *Int. J. Heat Mass Transf.* **42** (1999) 2357.
26. Y. Shabany and P. Durbin, *AIAA J.* **35** (1997) 985.
27. P. Wikstrom, S. Wallin and A. Johansson, *Phys. Fluids* **12** (2000) 688.
28. S. Lyons and T. Hanratty, *Int. J. Num. Meth. Fluids* **13** (1991) 999.
29. D. Papavassiliou and T. Hanratty, *Int. J. Heat Mass Transf.* **40** (1997) 1303.
30. V. Edwards and J. Newman, *J. Electrochem. Soc.* **134** (1987) 1181.
31. F.B.C.F. Wallgren, and B.J. Andersson, *Electrochim. Acta* **41** (1996) 2909.
32. J. Son and T. Hanratty, *AIChE J.* **13** (1967) 689.
33. W. Parrish and J. Newman, *J. Electrochem. Soc.* **117** (1970) 43.

Appendix

A. *k—ω model*

Wilcox [3] gives the following version of the 'Low-Reynolds' *k—ω* model. The *k—ω* model describes the turbulent kinetic energy k and the dissipation of turbulent kinetic energy per volume and time unit (ω) governed by the equations:

$$\frac{\partial k}{\partial t} + U_j \frac{\partial k}{\partial x_j} = \tau_{ij} \frac{\partial U_i}{\partial x_j} - \beta^* k\omega + \frac{\partial}{\partial x_j}\left[(\nu + \sigma^* \nu_t)\frac{\partial k}{\partial x_j}\right] \tag{28}$$

and

$$\frac{\partial \omega}{\partial t} + U_j \frac{\partial \omega}{\partial x_j} = \alpha \frac{\omega}{k} \tau_{ij} \frac{\partial U_i}{\partial x_j} - \beta \omega^2 + \frac{\partial}{\partial x_j}\left[(\nu + \sigma \nu_t)\frac{\partial \omega}{\partial x_j}\right] \tag{29}$$

The closure equations are as follows:

$$\nu_t = \alpha^* \frac{k}{\omega} \tag{30}$$

$$Re_t = \frac{k}{\nu\omega} \tag{31}$$

$$\alpha^* = \frac{\alpha_0^* + Re_t/R_k}{1 + Re_t/R_k} \tag{32}$$

$$\alpha = \frac{13}{25} \times \frac{\alpha_0 + Re_t/R_\omega}{1 + Re_t/R_\omega} \times (\alpha^*)^{-1} \tag{33}$$

$$\beta^* = \beta_0^* \times \frac{4/15 + (Re_t/R_\beta)^4}{1 + (Re_t/R_\beta)^4} \times f_{\beta^*} \tag{34}$$

$$\chi_k = \frac{1}{\omega^3}\frac{\partial k}{\partial x_j}\frac{\partial \omega}{\partial x_j}, \qquad \chi_\omega = \left|\frac{\Omega_{ij}\Omega_{jk}S_{ki}}{(\beta_0^*\omega)^3}\right| \tag{35}$$

$$f_{\beta^*} = 0, \qquad \chi_k \leqslant 0 \tag{36a}$$

$$f_{\beta^*} = \frac{1 + 680\chi_k^2}{1 + 400\chi_k^2}, \qquad \chi_k \geqslant 0 \tag{36b}$$

$$f_\beta = \frac{1 + 70\chi_\omega}{1 + 80\chi_\omega} \tag{37}$$

The mean rotation-rate tensor is defined by

$$\Omega_{ij} = \frac{1}{2}\left(\frac{\partial U_i}{\partial x_j} - \frac{\partial U_j}{\partial x_i}\right) \tag{38}$$

The closure coefficients are: $\beta_0^* = 9/100$, $\beta_0 = 9/125$, $\beta = \beta_0 f_\beta$, $\sigma^* = \sigma = 1/2$, $\alpha_0^* = 1/3\beta_0$, $\alpha_0 = 1/9$, $R_\beta = 8$, $R_k = 6$ and $R_\omega = 2.95$.

B. *Boundary conditions*

B.1. *Inlet*

At the inlet, the value of k and ω may be estimated based on the turbulent intensity I_{turb}:

$$k_{\text{inlet}} = \frac{3}{2}(I_{\text{turb}} v_{\text{inlet}})^2 \tag{39}$$

with v_{inlet} the velocity normal to the inlet. The turbulent intensity is the ratio of the fluctuating velocity over the average velocity. The higher the turbulent intensity the more turbulent the flow. A typical range for the turbulent intensity is about 1 to 5%.

Determining the initial ω requires some estimate of an appropriate length scale, l, typically 5% of the length of the inlet. From this we can the determine ω at the inlet to be:

$$\omega_{\text{inlet}} = \frac{k^{1/2}}{l} \tag{40}$$

The normal component of the velocity is imposed to the average velocity at the inlet; the tangential component is set to zero.

B.2. *Outlet*
A zero normal gradient (natural boundary condition) is assumed for the turbulent quantities at the outlet. A reference pressure is imposed.

B.3. *Walls*
For a nonmoving wall, the value of k and U_i are fixed at zero. For smooth walls, the value of ω is set to be

$$\omega_{\text{wall}} = \frac{6v}{\beta(\Delta y_{\text{wall}})^2} \tag{41}$$

where Δy_{wall} is the normal distance from the wall node to its nearest interior neighbour.